CHIN. PHYS. LETT. Vol. 38, No. 12 (2021) 127301

Effect of Geometrical Structure on Transport Properties of Silicene Nanoconstrictions

Yawen Guo(郭雅文)[1], Wenqi Jiang(蒋文琦)[1], Xinru Wang(王新茹)[1], Fei Wan(万飞)[1], Guanqing Wang(王关晴)[1*], G. H. Zhou(周光辉)[2], Z. B. Siu(萧卓彬)[3], Mansoor B. A. Jalil[3], and Yuan Li(李源)[1*]

[1]*Department of Physics, Hangzhou Dianzi University, Hangzhou 310018, China*
[2]*Department of Physics and Key Laboratory for Low-Dimensional Quantum Structures and Manipulation (Ministry of Education), Hunan Normal University, Changsha 410081, China*
[3]*Computational Nanoelectronics and Nano-device Laboratory, Electrical and Computer Engineering Department, National University of Singapore, Singapore 117576, Singapore*

(Received 21 September 2021; accepted 5 November 2021; published online 25 November 2021)

We study electrical modulation of transport properties of silicene nanoconstrictions with different geometrical structures. We investigate the effects of the position and width of the central scattering region on the conductance with increasing Fermi energy. It is found that the conductance significantly depends on the position and the width of the nanoconstriction. Interestingly, the symmetrical structure of the central constriction region can induce a resonance effect and significantly increase the system's conductance. We also propose a novel two-channel structure with an excellent performance on the conductance compared to the one-channel structure with the same total width. Such geometrically-induced conductance modulation of silicene nanostructures can be achieved in practice via current nanofabrication technology.

DOI: 10.1088/0256-307X/38/12/127301

Silicene has a low-buckling honeycomb structure formed from a monolayer of silicon atoms. After its recent successful synthesis on metal surfaces,[1−3] it has attracted much attention from both theoretical[4,5] and experimental researchers.[6,7] Its low-buckled geometry creates a relatively large bandgap induced by spin-orbit coupling at the Dirac points.[8] The most common substrate for silicene is the Ag(111) surface.[9,10] Silicene has stimulated the development of many related fields such as the valley-polarized quantum anomalous Hall effect,[11,12] quantum spin Hall effect,[13,14] spin and valley polarization,[15−18] and topologically protected edge states.[19,20] Specifically, researchers have attempted to control the energy band by applying an external electric field,[21] strain,[22] or a gate voltage.[23,24] Valley and spin separation can be achieved when a strain and an electric field are simultaneously applied to silicene.[25] However, effect of geometrical modulation in silicene devices has not been realized extensively. In this Letter, we discuss the effect of varying the position and width of the central scattering region as well as the external field and potential energy on the transport properties of the system.

Figure 1 shows a silicene nanoconstriction with one-channel (top) and two-channel (bottom) structures. In the one-channel structure, the central channel is displaced (blue region) by a distance of $\Delta y = M\xi$ along the y direction from the symmetrical position (orange region). M is an integer representing the number of sites in the shift, and $\xi = \frac{\sqrt{3}}{2}a = 3.34\,\text{Å}$, where $a = 3.86\,\text{Å}$ is the lattice constant. We calculate the conductance of the silicene nanoconstriction with both positive and negative values of M, and find that the results are dependent only on the absolute value of M and not its sign. This is due to the reflection symmetry of the geometric structure for positive and negative values of M with the same value of $|M|$. Therefore, we will only consider positive values of M and $M = 0$, i.e., $M = 0, 1, 2, 3, \ldots$. The length of the scattering region is 800 sites and the wide part has 40 sites, which translate to dimensions of $L \approx 153\,\text{nm}$, $W \approx 13\,\text{nm}$. The width of the central region is $D = (N-1)\xi + \frac{1}{4}a$, in which $N = 2, 3, 4, \ldots$ is the number of sites in the central narrow part.

We adopt the tight-binding Hamiltonian as follows:[8,26,27]

$$H = -\sum_{i\alpha} a_z \mu_i E_z c^\dagger_{i\alpha} c_{i\alpha} + \sum_{i\alpha} V_i c^\dagger_{i\alpha} c_{i\alpha} - \epsilon \sum_{\langle i,j\rangle\alpha} c^\dagger_{i\alpha} c_{j\alpha} + i\frac{t_{\text{SO}}}{3\sqrt{3}} \sum_{\langle\langle i,j\rangle\rangle\alpha\beta} \kappa_{ij} c^\dagger_{i\alpha} \sigma^z_{\alpha\beta} c_{j\beta}. \quad (1)$$

The first term is associated with the staggered sublattice potential due to the low-buckled structure with $a_z = 0.23\,\text{Å}$. In the summation, $\mu_i = 1$ ($\mu_i = -1$) denotes the A (B) sites and $c^\dagger_{i\alpha}$ ($c_{i\alpha}$), the creation (annihilation) operator with spin index α at site i. The

Supported by the National Natural Science Foundation of China (Grant No. 11574067).
*Corresponding authors. Email: gqwang@hdu.edu.cn; liyuan@hdu.edu.cn
© 2021 Chinese Physical Society and IOP Publishing Ltd

second term is the on-site potential energy induced by gate voltage. The third term describes the hopping of the nearest neighbors with $\epsilon \approx 1.09\,\text{eV}$. The summation indices $\langle i,j\rangle$ and $\langle\langle i,j\rangle\rangle$ denote summations over the nearest- and next-nearest-neighbor hopping sites, respectively. The fourth term represents the effective spin-orbit coupling. The coupling coefficient is $t_{\text{SO}} \approx 3.9\,\text{meV}$, and $\boldsymbol{\sigma} = (\sigma_x, \sigma_y, \sigma_z)$ are the Pauli matrices. Here κ_{ij} takes the value of 1 (-1) for an anticlockwise (clockwise) hopping with respect to the positive direction of the z axis.

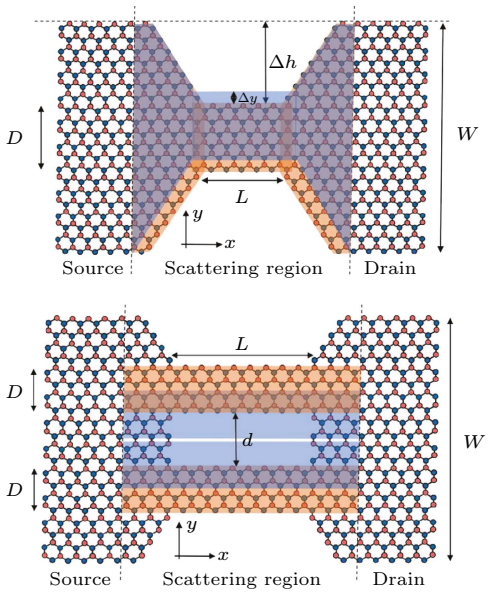

Fig. 1. Schematic of the silicene nanoconstriction with one-channel (top) and two-channel (bottom) structures. Here $d = 2M\xi$ in the two-channel structure is the distance between two central nanoribbons.

The conductance can be calculated by the Landauer–Büttiker formula:[28,29]

$$G = \frac{e^2}{h}\sum_{mn}|t_{n,m}|^2. \tag{2}$$

Here, $t_{n,m}$ represents the transmission amplitude from mode m to n; $t_{n,m}$ can be written as

$$t_{n,m} = \tilde{\psi}^{\dagger}_{\text{R},n}(+)G_{S+1,0}[G^{(0)}_{0,0}]^{-1}\psi_{\text{L},m}(+), \tag{3}$$

where $\psi_{\text{R/L},n}(+)$ is the nth right-going propagating mode of the right (left) lead, $\tilde{\psi}_{\text{R/L},n}(+)$ is its dual vector. $G^{(0)}_{0,0}$ and $G_{S+1,0}$ are Green's functions of the left lead and the full system, respectively. The Green functions $G^{(0)}_{0,0}$ and $G_{S+1,0}$ can be obtained using the iterative Green function method.[30]

We mainly investigate the effects of structural changes such as the position and width of the central scattering region combined with the electric field and potential energy on the transport properties. We first discuss the dispersion relationship of silicene with zigzag edges. Figure 2(a) shows the band structures of the lead (left) and the central scattering region (right) with the electrical field $E_z = 0$ and $V_0 = 0.3\,\text{eV}$. It can be seen from Fig. 2(b) that when $E_z = 0.5\,\text{eV/Å}$, a band gap will emerge. Thus the band structure and gap can be changed by the potential energy and electric field.

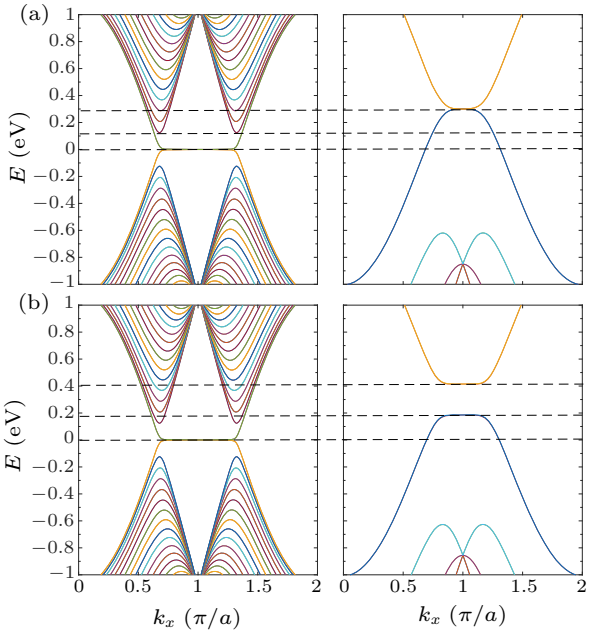

Fig. 2. The band structure of the lead (left) and the central scattering region (right) with the electric fields (a) $E_z = 0$ and (b) $E_z = 0.5\,\text{eV/Å}$. The potential energy $V_0 = 0.3\,\text{eV}$ and the number of sites in the central narrow part is $N = 4$.

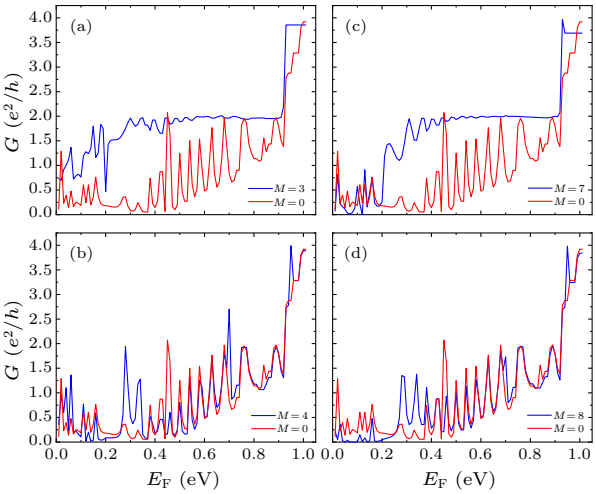

Fig. 3. The conductance G for different values of the Fermi energy without an external electric field and potential energy when the vertical displacement of the central part is (a) $M = 3$, (b) $M = 4$, (c) $M = 7$, and (d) $M = 8$ sites. The number of sites in the central nanoribbon is $N = 4$.

Next, we study the influence of the position of the central nanoribbon on the transport properties with and without external field effects. In Fig. 3, the conductance is plotted as a function of Fermi energy E_{F}

when the central narrow part is at different positions. The width of central nanoribbon is 4 sites, that is $N = 4$. When the displacement is 3 sites ($M = 3$), the conductance first oscillates with increasing Fermi energy before it stabilizes when the Fermi energy reaches 0.5 eV. There is a step near 0.94 eV, above which a new conductance plateau with $G \approx 3.75\ e^2/h$. It can be seen that the trends shown by the overall conductance change significantly compared to the case where the nanoribbon remains at the center, i.e., when $M = 0$. When the displacement is over 4 sites ($M = 4$), no stable conductance plateau is formed. There is an energy region with small conductance approaching to zero for energies near 0.2 eV, which can be attributed to the interference between propagating modes and the mode matching between the narrow and wide regions.

However, when the vertical displacement of the central nanoribbon is further increased to 7 sites ($M = 7$), a stable conductance plateau of $2e^2/h$ reemerges between 0.5 eV and 0.94 eV of Fermi energy. This stable plateau disappears when the vertical displacement of the scattering region is adjusted to 8 sites ($M = 8$) off the center. The results in Fig. 3 can be summarized as follows: At odd values of the vertical displacement M, the conductance profile exhibits a stable conductance plateau, whereas at even values of M, the interference and the mode-matching effect induce zero conductance within the energy regime 0–0.2 eV, as shown in Fig. 3(d). When M is even, conductance oscillations arise from the interference between the left-going and right-going modes for $0.5 < E_{\rm F} < 0.94$ eV. However, when the displacement of the narrow part is odd ($M = 3$ or 7), the interference is broken because of the asymmetrical structure, and the oscillating peaks disappear. Accordingly, the conductance becomes a stable plateau between $0.5 < E_{\rm F} < 0.94$ eV. It is interesting that the nanoconstriction has different transport properties between odd- and even-numbered vertical displacements from the center. We also conduct a series of calculations for other values of M and obtain the same phenomenon. Some previously published works reported that zigzag silicene nanoribbons with even and odd widths have very different current-voltage relationships, magnetoresistance and thermopower behavior, and these differences were attributed to the different parities of their π and $\pi^\star$ bands.[31,32] However, our results further point out that the even-M and odd-M positions of central nanoribbons with the same width also have very different transport properties. This difference can be explained by noting that the even-M and odd-M cases result in two distinct types of interfaces between the wide and narrow segments with different atomic configurations. Hence the two cases give rise to two different classes of conductance behavior. Within each class, one observes that the conductance profiles are similar and change more smoothly as a function of the displacement magnitude.

We further investigate the combined influence of the electric field and the potential energy. As shown in Fig. 4, the conductance exhibits several peaks when the Fermi energy is below 0.19 eV and remains zero at Fermi energies between 0.19 eV and 0.41 eV in all the conductance profiles, in sharp contrast to the profiles in Fig. 3. The conductance gap appears because the electrical field opens a band gap, as shown in Fig. 2(b). When the Fermi energy is larger than 0.41 eV, these conductance profiles again exhibit the differing behaviors between the even-M and odd-M cases. The conductance has an apparent step when the displacement is an odd number of sites. The step structure exhibits obvious oscillated behaviors above $E_{\rm F} = 0.5$ eV compared with the plateau shown in Fig. 3. The difference between two steps can attribute to different interferences because the potential energy V_0 can result in an n-p-n-type heterojunction. However, the conductance of the even-M shift exhibits a dip of about 50% at slightly below 0.6 eV, forming a pothole-like pattern, as well as greater fluctuations before gradually increasing and becoming stable around 1.75 e^2/h. Although the conductances of the four patterns all oscillate, the oscillation amplitude is significantly larger when the value of M is even. Moreover, the overall conductance in the nanoconstrictions with odd values of M is larger than that in the cases with even shifts.

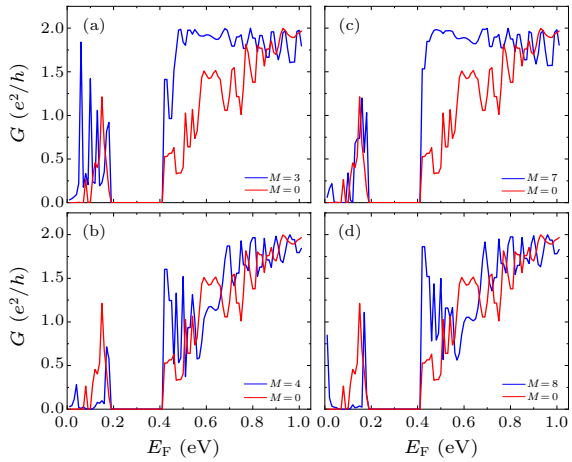

Fig. 4. The conductance G for different values of the Fermi energy with external electric field $E_z = 0.5$ eV/Å and potential energy $V_0 = 0.3$ eV when the vertical displacement of the central part is (a) $M = 3$, (b) $M = 4$, (c) $M = 7$, and (d) $M = 8$ sites. The number of sites in the central nanoribbon is $N = 4$.

Next, we change the width of central nanoribbon and then calculate its transmission at the electric field of $E_z = 0.5$ eV/Å and potential energy of $V_0 = 0.3$ eV (note that for odd values of N, the narrow nanoribbon was positioned such that the top edge of the narrow nanoribbon is located at ceil$(N/2) + M$ sites above the center of the wide nanoribbon). As we broaden

the width of the scattering region, we find that the characteristic of the transport property has some important changes. The most intuitive change is that all the conductance profiles exhibit distinct step-like shape regardless of whether M is odd or even, unlike panels (b) and (d) in Figs. 3 and 4 where obvious steps are not clearly discernable. We also note that the behavior of the odd-even site vertical displacement of the central segment seems to have a reversed effect on the conductance compared to that of Figs. 3 and 4. As shown in Fig. 5, the steps are more stable in the even-M case instead, especially at the smaller values of N. The larger stability in the even-M case can be seen from the fact that when the width is 5 and 6 sites [Figs. 5(a), 5(b)] and M is odd, the conduction profiles show the pothole-like conduction dips which appear in Fig. 4 where the width is 4 sites and M is even instead. As the width increases from $N = 5$ to $N = 8$, the pothole-like conduction dips become narrower and shallower, and finally a step pattern similar to the odd-M case can form. This illustrates that the odd-even effect of M is weakened as the width increases. In addition, when Fermi energy is greater than 0.41 eV, the conductance of the silicene heterojunction becomes more stable as the width increases.

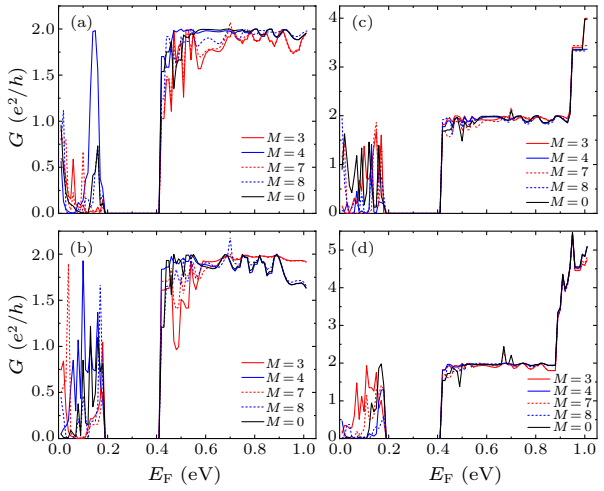

Fig. 5. The conductances are plotted as a function of the Fermi energy for different widths and vertical displacements of the central nanoribbon. The width is (a) 5 sites ($N = 5$), (b) 6 sites ($N = 6$), (c) 7 sites ($N = 7$) and (d) 8 sites ($N = 8$). The other parameters are $E_z = 0.5\,\text{eV/Å}$ and $V_0 = 0.3\,\text{eV}$.

How can this reversal in the even-odd M conductance profiles of the system with an increase in the width of the central segment be explained? Recall that the width of the wide nanoribbon is 40 sites. The distance between the top edges of the narrow and wide nanoribbon regions Δh is related to the transverse displacement of the narrow M by $\Delta h = 20 - \text{ceil}(N/2) - M$. Therefore, for $N = 4$, Δh is odd when M is odd. For example, when $M = 3$, $\Delta h = 15$ sites. However, when the number of sites in the central nanoribbon is $N = 5$ and $M = 0$, there are 3 sites above the transverse center of the wide nanoribbon leads and 2 sites beneath the center. Therefore, when the shift parameter M is odd, Δh is even. Finally, when $N = 6$, Δh is even when M is odd. Because we only consider the upward shift of the central region, the sum of the number of sites in the central region above the transverse center at $M = 0$ in combination with the shift M will determine the parity of Δh. Based on the above results, we find that the differing behaviors of the conductance profiles are consistent with the parity of Δh. In order to verify our speculation, we adopt the structure with 2 sites of width above the transverse center and 3 sites beneath the center at $M = 0$ and calculate the resulting transport properties. The obtained results show that when the Δh is odd, the step-like conductance pattern is indeed more stable. As the width of the central region increases, the difference between the parities gradually decreases, and steps emerge in the conductance patterns. Therefore, it can be further revealed from the figure that when the width D is small, the conductance of odd-Δh structure is more stable than the even-Δh case. As the width D of the central region increases, the pothole pattern gradually disappears and the odd-even effect of Δh disappears.

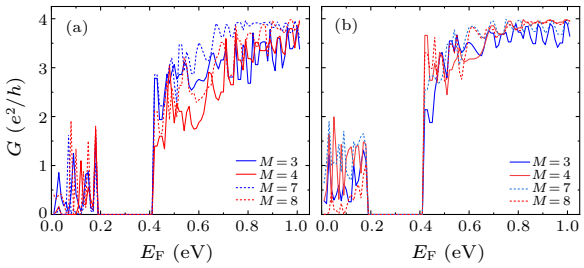

Fig. 6. The conductances are plotted as a function of Fermi energy in the structure of two channels. The width of each channel is (a) 3 sites ($N = 2 \times 3$), (b) 4 sites ($N = 2 \times 4$). The other parameters are $E_z = 0.5\,\text{eV/Å}$ and $V_0 = 0.3\,\text{eV}$.

We finally investigate the transmission across a novel structure for the central scattering region. As shown in the lower panel of Fig. 1, the central region is divided into two symmetrical parts along the transverse direction. When the two central nanoribbons are separated, the total width of the central region is given by $2D = (2N - 2)\xi + \frac{1}{2}a$, in which $2N = 4, 6, 8, \ldots$ is the total number of sites in the two nanoribbons. The distance between two channels is denoted as $d = 2M\xi$. When $d = 0$, as shown by the blue region, the situation is the same as that of the one-channel nanoconstrictions. Here, we only consider the symmetrical displacement of the two nanoribbons from their original position of $d = 0$ along the positive and negative directions of the y-axis. Totally different transport properties, as shown in Fig. 6, are obtained when the one-channel of scattering region is expanded into two

channels.

It can be seen that in this structure, the entire silicene heterojunction is symmetrical in the transverse direction. We choose the total widths of $N = 2 \times 3$ and $N = 2 \times 4$ for analysis. The width of each channel in the nanoribbon is 3 sites in Fig. 6(a) and 4 sites in Fig. 6(b). Under the conditions of $V_0 = 0.3\,\text{eV}$ and $E_z = 0.5\,\text{eV/Å}$, the distance between the two channels is changed. As shown in Fig. 6, the two-channel nanoconstrictions have similar step-like transmission profiles as those of the one-channel nanoconstrictions. However, the maximum value of the conductance in the two-channel silicene nanoconstriction is almost twice of the one-channel nanoconstriction with the same total width. For example, the maximum conductance of the center scattering region with $N = 8$ [shown in Fig. 5(d)] is only about half the value in the two-channel structure with $N = 2 \times 4$ [as shown in Fig. 6(b)]. The two-channel structure results in an obvious enhancement of the conductance.

In summary, we have studied the influence of the geometric structure of the silicene nanoconstriction on the transport properties. When there is no potential energy and electric field, a vertical displacement of the central nanoribbon by an odd number of sites will stabilize the conductance over some values of the Fermi energy, while a displacement by even number of sites will not produce such a flat conductance plateau. When an external electric field and gate potential are applied, the abrupt change of the conductance for odd-M produces a step-like conductance profile, while the conductance for even-M oscillates and rises gradually. We have also studied the variation of the conductance with the width of the scattering region. The step conductance profile is affected by whether Δh is even or odd, which becomes more stable when Δh is odd. The stability of the step increases with the width of the nanoribbon. We investigate a novel two-channel structure and find that its conductance is almost twice the value of a one-channel structure with the same total width. Thus, variation in the silicene nanoconstriction even at the atomic length scale can produce a profound change to the transport across the nanoconstriction. From the experimental point of view, such variation of the width and position of the nanoconstriction at the atomic resolution are expected to be achieved by nanofabrication techniques such as focused ion beam.[33,34]

References

[1] Aufray B, Kara A, Vizzini S, Oughaddou H, Léandri C, Ealet B and Lay G L 2010 *Appl. Phys. Lett.* **96** 183102
[2] Lalmi B, Oughaddou H, Enriquez H, Kara A, Vizzini S, Ealet B and Aufray B 2010 *Appl. Phys. Lett.* **97** 223109
[3] De Padova P, Quaresima C, Ottaviani C, Sheverdyaeva P M, Moras P, Carbone C, Topwal D, Olivieri B, Kara A and Oughaddou H 2010 *Appl. Phys. Lett.* **96** 261905
[4] Cahangirov S, Topsakal M, Aktürk E, Şahin H and Ciraci S 2009 *Phys. Rev. Lett.* **102** 236804
[5] Fagan S B, Baierle R J, Mota R, Silva A J R D and Fazzio A 2000 *Phys. Rev. B* **61** 9994
[6] Chen L, Liu C C, Feng B J, He X Y, Cheng P, Ding Z J, Meng S, Yao Y G and Wu K H 2012 *Phys. Rev. Lett.* **109** 056804
[7] Vogt P, De Padova P, Quaresima C, Avila J, Frantzeskakis E, Asensio M C, Resta A, Ealet B and Lay G L 2012 *Phys. Rev. Lett.* **108** 155501
[8] Liu C C, Jiang H and Yao Y G 2011 *Phys. Rev. B* **84** 195430
[9] Guo Z X, Furuya S, Iwata J and Oshiyama A 2013 *Phys. Rev. B* **87** 235435
[10] Lin C L, Arafune R, Kawahara K, Kanno M, Tsukahara N, Minamitani E, Kim Y, Kawai M and Takagi N 2013 *Phys. Rev. Lett.* **110** 076801
[11] Ezawa M 2012 *New J. Phys.* **14** 033003
[12] Pan H, Li Z S, Liu C C, Zhu G B, Qiao Z H and Yao Y G 2014 *Phys. Rev. Lett.* **112** 106802
[13] Liu C C, Feng W X and Yao Y G 2011 *Phys. Rev. Lett.* **107** 076802
[14] Tabert C J and Nicol E J 2013 *Phys. Rev. B* **87** 235426
[15] Missault N, Vasilopoulos P, Vargiamidis V, Peeters F M and Van Duppen B 2015 *Phys. Rev. B* **92** 195423
[16] Stille L, Tabert C J and Nicol E J 2012 *Phys. Rev. B* **86** 195405
[17] Yesilyurt C, Tan S G, Liang G and Jalil M B A 2015 *Appl. Phys. Exp.* **8** 105201
[18] Siu Z B and Jalil M B A 2021 *Sci. Rep.* **11** 7575
[19] Ezawa M and Nagaosa N 2013 *Phys. Rev. B* **88** 121401(R)
[20] Cano-Cortes L, Ortix C and van den Brink J 2013 *Phys. Rev. Lett.* **111** 146801
[21] Van Duppen B, Vasilopoulos P and Peeters F M 2014 *Phys. Rev. B* **90** 035142
[22] Li Y, Jiang W Q, Ding G Y, Peng Y Z, Wen Z C, Wang G Q, Bai R, Qian Z H, Xiao X B and Zhou G H 2019 *J. Appl. Phys.* **125** 244304
[23] Yamakage A, Ezawa M, Tanaka Y and Nagaosa N 2013 *Phys. Rev. B* **88** 085322
[24] Guzmán E, Navarro O, Oubram O and Rodríguez-Vargas I 2018 *J. Appl. Phys.* **124** 144305
[25] Li Y, Zhu H B, Wang G Q, Peng Y Z, Xu J R, Qian Z H, Bai R, Zhou G H, Yesilyurt C, Siu Z B and Jalil M B A 2018 *Phys. Rev. B* **97** 085427
[26] Kane C L and Mele E J 2005 *Phys. Rev. Lett.* **95** 146802
[27] Ezawa M 2012 *Phys. Rev. Lett.* **109** 055502
[28] Büttiker M, Imry Y, Landauer R and Pinhas S 1985 *Phys. Rev. B* **31** 6207
[29] Wimmer M 2009 *PhD Dissertation* (German: University of Regensburg)
[30] Khomyakov P A, Brocks G, Karpan V, Zwierzycki M and Kelly P J 2005 *Phys. Rev. B* **72** 035450
[31] Kang J, Wu F and Li J 2012 *Appl. Phys. Lett.* **100** 233122
[32] Zhou B L, Zhou B H, Chen X W, Liao W H and Zhou G H 2015 *J. Phys.: Condens. Matter* **27** 465301
[33] Khizroev S, Hijazi Y, Chomko R, Mukherjee S, Chantrell R, Wu X, Carley R and Litvinov D 2005 *Appl. Phys. Lett.* **86** 042502
[34] Fernández-Pacheco A, De Teresa J M, Córdoba R and Ibarra M R 2008 *Nanotechnology* **19** 415302